Biomaterials Advances 153 (2023) 213563

Contents lists available at ScienceDirect

Biomaterials Advances

journal homepage: www.journals.elsevier.com/materials-science-and-engineering-c

Layer-by-layer coated calcium carbonate nanoparticles for targeting breast cancer cells

Filipa R. Bastos, Diana Soares da Costa, Rui L. Reis, Natália M. Alves, Iva Pashkuleva *, Rui R. Costa *

3B's Research Group, I3Bs – Research Institute on Biomaterials, Biodegradables and Biomimetics, University of Minho, Headquarters of the European Institute of Excellence on Tissue Engineering and Regenerative Medicine, AvePark, Parque de Ciência e Tecnologia, Zona Industrial da Gandra, 4805-017 Barco, Guimarães, Portugal

ICVS/3B's – PT Government Associate Laboratory, Braga/Guimarães, Portugal

ARTICLE INFO

Keywords:
Layer-by-layer
Calcium carbonate
Hyaluronic acid
Breast cancer
Drug delivery

ABSTRACT

Breast cancer is resistant to conventional treatments due to the specific tumour microenvironment, the associated acidic pH and the overexpression of receptors that enhance cells tumorigenicity. Herein, we optimized the synthesis of acidic resorbable calcium carbonate ($CaCO_3$) nanoparticles and the encapsulation of a low molecular weight model molecule (Rhodamine). The addition of ethylene glycol during the synthetic process resulted in a particle size decrease: we obtained homogeneous $CaCO_3$ particles with an average size of 564 nm. Their negative charge enabled the assembly of layer-by-layer (LbL) coatings with surface-exposed hyaluronic acid (HA), a ligand of tumour-associated receptor CD44. The coating decreased Rhodamine release by two-fold compared to uncoated nanoparticles. We demonstrated the effect of nanoparticles on two breast cancer cell lines with different aggressiveness – SK-BR-3 and the more aggressive MDA-MB-231 – and compared them with the normal breast cell line MCF10A. $CaCO_3$ nanoparticles (coated and uncoated) significantly decreased the metabolic activity of the breast cancer cells. The interactions between LbL-coated nanoparticles and cells depended on HA expression on the cell surface: more particles were observed on the surface of MDA-MB-231 cells, which had the thickest endogenous HA coating. We concluded that $CaCO_3$ nanoparticles are potential candidates to carry low molecular weight chemotherapeutics and deliver them to aggressive breast cancer sites with an HA-abundant pericellular matrix.

1. Introduction

Breast cancer is one of the most malignant diseases among women. In 2020, 11.7 % of all diagnosed cancers were female breast cancer, making it the most prevalent cancer type in the world, followed by lung (11.4 %) and colorectal (10.0 %) [1]. There are different subtypes of breast cancer that are categorized according to the expression of three typical hormone receptors: oestrogen receptor (ER), progesterone receptor (PR), and human epidermal growth factor receptor-2 (HER2) [2–4]. Luminal A breast cancer is ER and PR positive; luminal B breast cancer is ER positive and depends on the HER2 status; and triple-negative breast cancer (TNBC) is the most aggressive subtype, in which none of these typical receptors are expressed. Currently, several treatments are clinically used but they all have limitations: i) chemotherapy, which consists in the administration of anticancer drugs, fails when tumours acquire drug resistance [5]; ii) radiotherapy uses radiation to kill tumorigenic cells but it is unselective and affects healthy cells as well [6]; iii) hormone treatments targeting the typical breast cancer markers can be less effective than chemotherapy and are not applicable in the case of TNBC [7,8].

The efficiency of the treatment can be improved if the therapy addresses the complexity of the tumour microenvironment (TME), especially in tumours that develop resistant and aggressive phenotypes. In breast cancer tumours, a high glycolytic cell metabolism results in the acidification of the TME to a pH of 6.3–6.9 [9–11]. Calcium carbonate ($CaCO_3$) is an inorganic and biocompatible material that is stable at neutral pH but dissolves in acids [12–14]. $CaCO_3$ particles can be obtained by fast, effective and affordable methods that involve the co-precipitation of calcium and carbonate ions in aqueous solutions. Proteins and other molecules can be added to the reaction medium and

* Corresponding authors.
E-mail addresses: pashkuleva@i3bs.uminho.pt (I. Pashkuleva), rui.costa@i3bs.uminho.pt (R.R. Costa).

https://doi.org/10.1016/j.bioadv.2023.213563
Received 9 May 2023; Received in revised form 10 July 2023; Accepted 17 July 2023
Available online 20 July 2023

encapsulated in $CaCO_3$ particles with high efficiency [15–17]. For example, doxorubicin, an anticancer drug, can be encapsulated in $CaCO_3$ particles and released in a pH-responsive manner: this drug is released 20 times faster in an acidic environment than at a neutral pH [18]. As endolysosomes have an acidic pH that can cause $CaCO_3$ resorption inside cells [19], $CaCO_3$ particles are promising candidates for cancer treatments.

$CaCO_3$ particles are negatively charged and thus can be used as templates for electrostatic-driven layer-by-layer (LbL) coating – an alternating deposition of oppositely charged building blocks onto a substrate [20–22]. The LbL method discards the need for chemical modification and the use of aggressive solvents. The deposition can be performed on substrates of any geometry under mild conditions (temperature, pressure, and pH), therefore enabling the use of sensitive, bioactive blocks that can enhance the efficiency of drug encapsulation and delivery to eukaryotic cells and bacteria [23,24].

In this work, we optimized the synthesis of $CaCO_3$ nanoparticles and their modification by LbL coating. To this end, we chose polyanionic hyaluronic acid (HA) as a bioactive building block for the coatings. HA is a natural ligand of the CD44 receptor that is overexpressed in different cancers, including breast cancer. CD44 and HA interact *via* the basic arginines Arg41 and Arg78 of the receptor and the carboxyl groups of HA [25]. Accumulation of HA in TME and overexpression of CD44 by cancer cells are associated with high invasiveness, stemness, and metastatic potential [26–28]. Previous studies with LbL films containing HA have demonstrated the utility of these constructs in understanding and manipulating the interactions between HA and CD44 [29,30]. Herein, we investigated the potential of pH-sensitive $CaCO_3$ nanoparticles LbL-coated with HA to target breast cancer cells with varying metastatic potential, and the effect of CD44 expression on its efficiency.

2. Materials and methods

2.1. Materials

Calcium chloride anhydrous ($CaCl_2$), heparin sodium salt from porcine intestinal mucosa (Hep, grade I-A, ≥180 USP units/mg), sodium chloride (NaCl), poly-L-lysine hydrobromide (PLL, molecular weight 15–30 kDa, determined by viscosity), rhodamine B isothiocyanate (Rho), antibiotic antimycotic solution (100×, stabilized with 10,000 units penicillin and 10 mg streptomycin), phosphate buffered saline (PBS, in tablets), potassium chloride (KCl), sodium phosphate dibasic (Na_2HPO_4), sodium phosphate monobasic (NaH_2PO_4), Dulbecco's Modified Eagle Medium (DMEM) high glucose with 4500 mg•L^{-1} glucose, L-glutamine, and sodium bicarbonate, without sodium pyruvate were purchased from Sigma-Aldrich (St. Louis MO, USA). Sodium carbonate anhydrous (Na_2CO_3, calcein AM, and trypsin/EDTA (0.05 % trypsin/0.53 mM EDTA) were purchased from VWR (Carnaxide, Portugal). Sodium hyaluronate (21–40 kDa) was purchased from Lifecore Biomedical (Chaska MN, USA). Ethylene glycol (>99.5 %, for analysis) was purchased from Carlo Erba (Val de Reuil, France). Foetal bovine serum (FBS, qualified, one-shot format), propidium iodide, and wheat germ agglutinin (WGA) labelled with fluorescein isothiocyanate (FITC) were purchased from Alfagene (Carcavelos, Portugal). Deep Blue Cell Viability™ kit was purchased from Lusopalex (Oeiras, Portugal). Anti-CD44 antibodies KM201 were obtained from Abcam (Cambridge UK).

2.2. Synthesis of calcium carbonate particles

$CaCO_3$ particles were synthesized by $CaCl_2$ and Na_2CO_3 co-precipitation at different conditions (Appendix, Fig. A.1). 5 M $CaCl_2$ and 1 M Na_2CO_3 solutions were prepared in distilled water. An aliquot of 650 μL of $CaCl_2$ solution was diluted with 125 μL of distilled water, followed by the addition of 2.5 mL Na_2CO_3 solution and stirring at 650 rpm for 16 h. Then, we added 5 mL of distilled water and stopped the agitation after 5 min. The particles were collected after centrifugation (1500 rpm, 3 min), and washed by resuspending them in 9 mL of ultrapure water, followed again by centrifugation. For the preparation of heparin-doped $CaCO_3$ (*i.e.,* Hep-$CaCO_3$), the method was adapted from Ueno et al. [31]. Briefly, in the above-described method, instead of the 125 μL of distilled water we used Hep solutions with concentrations ranging from 0.038 to 4.77 mg•mL^{-1} (Appendix, Fig. A.2, Table A.1). Hep-$CaCO_3$ loaded with Rho was produced by adding Rho to the Hep solution at a concentration of 100 μg•mL^{-1}. The method to prepare $CaCO_3$ in ethylene glycol (*i.e.,* EG-$CaCO_3$) was adapted from Parakhonskiy et al. [32]. 1 M Na_2CO_3 and 0.4 M $CaCl_2$ were first prepared in distilled water. For each solution, 1 mL was added to 10 mL of 1:5 H_2O: EG mixtures. Then, the mixture containing $CaCl_2$ was poured into the Na_2CO_3 mixture under agitation (600 rpm) and stopped after 30 s, 1 h, 1 h 30 min, 2 h, 3 h, 4 h and 24 h (Appendix, Fig. A.3, Table A.2). EG-$CaCO_3$ was also loaded with Rho by adding 1 mL of 100 μg•mL^{-1} Rho to the solution of Na_2CO_3. After the reaction, the particles were centrifuged (1500 rpm, 3 min) and washed with 22 mL of ultrapure water (23 mL if Rho was added) – followed again by centrifugation – to remove free Rho, EG, and salts.

2.3. Characterization of calcium carbonate particles

The size of $CaCO_3$, Hep-$CaCO_3$, and EG-$CaCO_3$ particles was determined by dynamic light scattering (DLS, Malvern Nano-ZS equipment, UK) with a He—Ne laser at an angle of 173° and polystyrene disposable cuvettes. Prior to the analysis, the particles were resuspended in water (same volume as the one used for the washing) and an aliquot of 1 mL was added in the cuvette. At these conditions, the count rate was between 300 and 500 kcps. The polydispersity index (PDI), the size distribution, and the z-average diameter were determined by fitting the correlation function with the cumulant method (Zetasizer Nano v7.10 software). The experiments were done in quintuplicate. Dry particles were observed by a scanning electron microscope (SEM, JEOL-JSM-6010LV, Tokyo, Japan). After preparation, the particles were centrifuged for 3 min at 1500 rpm and washed in ultrapure water. A 100 μL drop of each formulation was dispensed on glass, placed on a SEM holder, and left to dry for 24 h at 37 °C. The particles were then sputtered with gold and placed in the SEM sample chamber.

2.4. Layer-by-layer coating of calcium carbonate particles

EG-$CaCO_3$ nanoparticles were washed with 0.15 M NaCl and suspended alternately in 2 mg•mL^{-1} solutions of PLL and HA prepared in 0.15 M NaCl under mild agitation (250 rpm) for 10 min. Each deposition step was intercalated with a washing step in 0.15 M NaCl, and for each deposition/washing step the nanoparticles were retrieved from suspension by low-speed centrifugation (1500 rpm, 3 min). The supernatant was removed with the aid of a micropipette and replaced by the next coating/washing solution. The procedure was repeated until 3 PLL/HA bilayers were assembled. The deposition of each polyion was followed by measuring the zeta (ζ)-potential of the nanoparticles using folded capillary cuvettes and the Nano-ZS equipment (Malvern, UK). The measurements were performed in triplicate.

2.5. In vitro release of rhodamine

To ensure sink conditions, EG-$CaCO_3$ nanoparticles (200 mg) were placed in flat-bottom polypropylene vials with 12 mL of PBS solution with pH 7.4 or pH 6.3 (140 mM NaCl, 3 mM KCl, 2 mM Na_2HPO_4, 8 mM NaH_2PO_4) and shaken (60 rpm) at 37 °C. The *in vitro* release of Rho from nanoparticles (uncoated and coated with one PLL/HA bilayer) was determined at 0 h, 1 h, 3 h, 1 day, 3 days, and 7 days using a sample-and-separate method [33–36] and quantification of encapsulated (*i.e.*, unreleased) Rho. Briefly, at each pre-determined time-point, the suspension was homogenized (pipetting up and down) and 400 μL aliquots

were collected. The particles from the aliquots were separated from the media by centrifugation (2 min, 10,000 rpm) and washed with ultrapure water several times to remove any free Rho. Then, 1 M HCl (3 mL) was added to dissolve the EG-$CaCO_3$ nanoparticles and the Rho amount was measured by a fluorescence spectrophotometer (JASCO model FP-8500, Tokyo, Japan) at an excitation wavelength of 564 nm (determined from the maximum absorbance peak of a 50 μg•mL^{-1} Rho solution (Appendix, Fig. A.4)) and emission interval between 575 nm and 650 nm. The intensity of the emitted fluorescence was read at 585 nm and compared to a calibration curve of known Rho concentrations (Appendix, Fig. A.5) to determine the mass of encapsulated Rho at each time-point (Q_{enc}). The experiments were performed in triplicate. The initial amount of Rho was determined at time-point "0 h" (Q_0) using the same particle dissolution method, resulting in approximately 260 ng of Rho. The cumulative release at each time-point (Q_{CR}) was calculated as a percentage of Q_0 using Eq. (1):

$$Q_{CR}(\%) = 100 - \left(\frac{Q_{enc}}{Q_0} \times 100\right) \quad (1)$$

The release profiles were fitted to several known drug release models [37]: zero-order (Appendix, Eq. A.1), first-order (Appendix, Eq. A.2), Higuchi release (Appendix, Eq. A.3), and Korsmeyer-Peppas (Appendix, Eq. A.4). The coefficients of determination (r^2) were calculated to find the model that best explained the experimental release profiles.

2.6. In vitro cell culture

MDA-MB-231 and SK-BR-3 epithelial breast cancer cell lines and a non-tumorigenic MCF10A breast epithelial cell line were obtained from the American Type Culture Collection (ATCC, Manassas VA, USA). For expansion, cells were routinely cultured on 75 cm^2 tissue culture polystyrene flasks with high glucose DMEM supplemented with 10 % FBS and 1 % antibiotics/antimycotics in an incubator at 37 °C and a humidified air atmosphere with 5 % CO_2. The medium was replaced every 2 or 3 days with fresh DMEM. When cells reached 80 % confluence, they were detached with 0.05 % trypsin/0.53 mM EDTA (37 °C, 5 % CO_2, 5 min). The trypsin was inactivated by adding complete medium, and the cells were centrifuged at 300 *g* for 5 min. Cells were resuspended in DMEM for a new expansion or transferred to well plates for incubation experiments with $CaCO_3$ nanoparticles. In the latter case, cells were first seeded in 48 well plates (15000 cells•cm^{-2}). After 24 h, approximately 4×10^8 uncoated or LbL-coated EG-$CaCO_3$ nanoparticles dispersed in 2.5 μL of PBS (pH 7.4) were added to each well containing 500 μL of medium and incubated for 1, 2 and 3 days at 37 °C and 5 % CO_2. All procedures, from the synthesis of nanoparticles to their coating, were performed in sterile conditions inside a laminar flow chamber and using filtered (cut-off 0.22 μm) solutions.

2.7. Metabolic activity and cell viability

Metabolic activity and Live/Dead assays were performed after predetermined culture periods (1, 2, and 3 days). Live/Dead assays were performed by staining living and dead cells with calcein AM (green) and propidium iodide (red), respectively. Stained cells were observed by a confocal laser scanning microscope (CLSM, Zeiss AiryScan 2 model LSM 980, Jena, Germany).

Metabolic activity was assessed by the Alamar Blue™ test. After 4 h of incubation, the fluorescence (F_{exp}) was measured using black 96-well plates ($\lambda_{ex} = 560$ nm; $\lambda_{em} = 590$ nm) and a microplate reader (Synergy HT, Bio-TEK, Santa Clara CA, USA). The reduction of Alamar Blue™ reagent (R_{AB}) was calculated following the supplier's instructions using Eq. (2):

$$R_{AB}(\%) = \frac{F_{exp} - F_{NC}}{F_{PC} - F_{NC}} \times 100 \quad (2)$$

where F_{NC} is the fluorescence of the negative control (*i.e.,* media containing Alamar Blue™ but no cells or particles) and F_{PC} is the fluorescence of the positive control (*i.e.,* media containing both the cells and Alamar Blue™ but no particles). Three independent experiments were performed and each condition was measured in triplicate. Metabolic activity is presented as a percentage of the positive control. Statistical significance between groups was determined by one-way ANOVA and compared using the Shapiro-Wilks test (GraphPad Prism version 8.0.1, San Diego CA, USA). The levels of significance for statistical differences were set to $p < 0.05$(*), $p < 0.01$(**), and $p < 0.001$(***).

2.8. $CaCO_3$ internalization with and without CD44 receptor blockage

The internalization of uncoated and LbL-coated EG-$CaCO_3$ nanoparticles was assessed 24 h, 48 h, and 72 h after the addition of the nanoparticles to the culture (CLSM, Zeiss AiryScan 2 model LSM 980, Jena, Germany). Rho is fluorescent in the red spectrum and allows visualization of the nanoparticles and determination of their localization. The distribution profiles of the Rho-loaded EG-$CaCO_3$ nanoparticles were plotted using the Fiji image processing package (v1.53t) [38], using the CLSM micrographs taken from the confocal plane of the middle of the cells. The red fluorescence intensity was calculated with background correction. To probe if the internalization is CD44-dependent, the CD44 receptors were blocked by a CD44 blocking antibody (KM201, Abcam). Twenty-four hours after seeding (15,000 cells•cm^{-2}) cell monolayers were incubated with 200 μL of complete DMEM supplemented with the CD44 blocking antibody (10 μg•mL^{-1}) at 37 °C in a 5 % CO_2 atmosphere. After 30 min, the cells were washed with PBS and nanoparticles were added, as previously described. Because HA plays important roles in TME, we also assessed the effect of the nanoparticles on HA expression (staining with labelled lectin FITC-WGA, green) and visualized the particles embedment within pericellular HA (CLSM, Zeiss AiryScan 2 model LSM 980, Jena, Germany).

To confirm the pericellular HA coating, MDA-MB-231 and SK-BR-3 cells were seeded on TCPS for 48 h and fixed with 10 % buffered formalin (1 h, 4 °C), and stained with biotinylated HA binding protein from bovine nasal cartilage (1 μg•mL^{-1}, 1 h at room temperature, Millipore) followed by incubation with streptavidin-AlexaFluor® 488 conjugate (1 μg•mL^{-1}, 10 min at room temperature, Molecular Probes). Images were acquired using an Inverted confocal microscope (TCS SP8, Leica Microsystems, Wetzlar, Germany). All microscopy visualization studies were performed with three independent specimens to confirm the reproducibility of the observations.

3. Results and discussion

3.1. Synthesis and characterization of calcium carbonate nanoparticles

The properties of $CaCO_3$ obtained by co-precipitation depend on the reaction conditions. Particles with different dimensions, shapes and crystallinities can be obtained from subtle changes in the time and velocity of agitation, Ca^{2+}/CO_3^{2-} ratios, and the addition of doping agents, among others [39]. When using a simple co-precipitation of $CaCl_2$ and Na_2CO_3 in water (*i.e.,* without any additives), $CaCO_3$ particles with diameters between 2 and 10 μm are obtained [40–42]. Recent studies suggest that $CaCO_3$ precipitation is slower when Ca^{2+} is in excess compared to CO_3^{2-} [43], which may result in the formation of smaller particles. We used a Ca^{2+}:CO_3^{2-} ratio of 5:1 and DLS in aqueous media showed the formation of $CaCO_3$ with a diameter of around 3.6 μm (Fig. 1A).

To decrease the particles size, we added a charged polymer to the precipitation medium to induce electrostatic repulsion between the $CaCO_3$ crystals during formation. We chose Hep because it is the natural polyelectrolyte with the highest negative charge and is already used in clinics [44,45]. We studied the influence of Hep concentration on the size of the particles (Appendix, Fig. A.2, Table A.1) and observed that

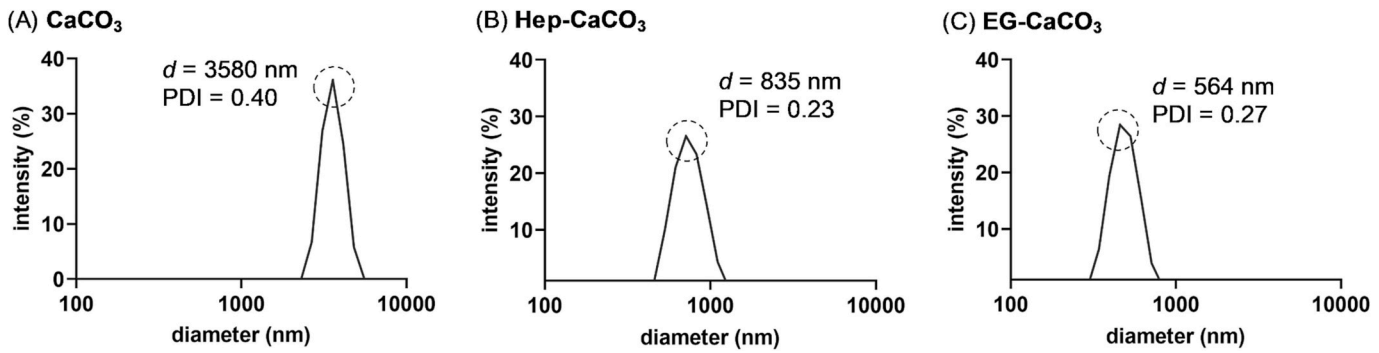

Fig. 1. Representative size distribution of (A) $CaCO_3$, (B) Hep-$CaCO_3$ and (C) EG-$CaCO_3$ determined by DLS. The values shown in the DLS graphs correspond to the diameter (*d*) and polydispersity index (PDI) of the distribution peak.

increasing the Hep quantity led to a systematic decrease of the particles size (diameter from 2.7 μm for 0.038 mg•mL^{-1} Hep to 835 nm for 4.77 mg•mL^{-1} Hep) and PDI (Fig. 1B). We also tested EG as an additive because previous studies have shown that EG can slow down the reaction and crystal growth [32]. To optimize the reaction time, we monitored the particles size for 24 h (Appendix, Fig. A.3, Table A.2). Within 2 h, we obtained monodisperse particles with a diameter around 564 nm (Fig. 1C), *i.e.,* in aqueous media EG-$CaCO_3$ nanoparticles were smaller than $CaCO_3$ and Hep-$CaCO_3$ particles. Because the obtained pure $CaCO_3$ particles were too large for our aim [46], we proceeded only with Hep-$CaCO_3$ and EG-$CaCO_3$ particles.

The capacity of Hep-$CaCO_3$ and EG-$CaCO_3$ particles to retain and release a cargo was investigated by encapsulating the fluorophore Rho (≈500 Da) as a model for low molecular weight substances (*e.g.,* therapeutics and small fluorescent probes). The amount of the encapsulated Rho in each system was quantified by dissolving the particles in 1 M HCl: we obtained 50.4 μg of Rho per mole of $CaCO_3$ in Hep-$CaCO_3$ and 130.5 μg per mole of $CaCO_3$ in EG-$CaCO_3$, *i.e.*, the amount of Rho was 3-fold higher in EG-$CaCO_3$ particles.

The effect of Rho on the morphology and size of Hep-$CaCO_3$ and EG-$CaCO_3$ was assessed by SEM and DLS analysis. Most unloaded Hep-$CaCO_3$ particles had sizes between 800 nm and 1.5 μm, and a rhombohedral morphology (Fig. 2A1 and Fig. A.6-i in the Appendix) – typical for calcite particles, one of the most stable $CaCO_3$ polymorphs [47]. The

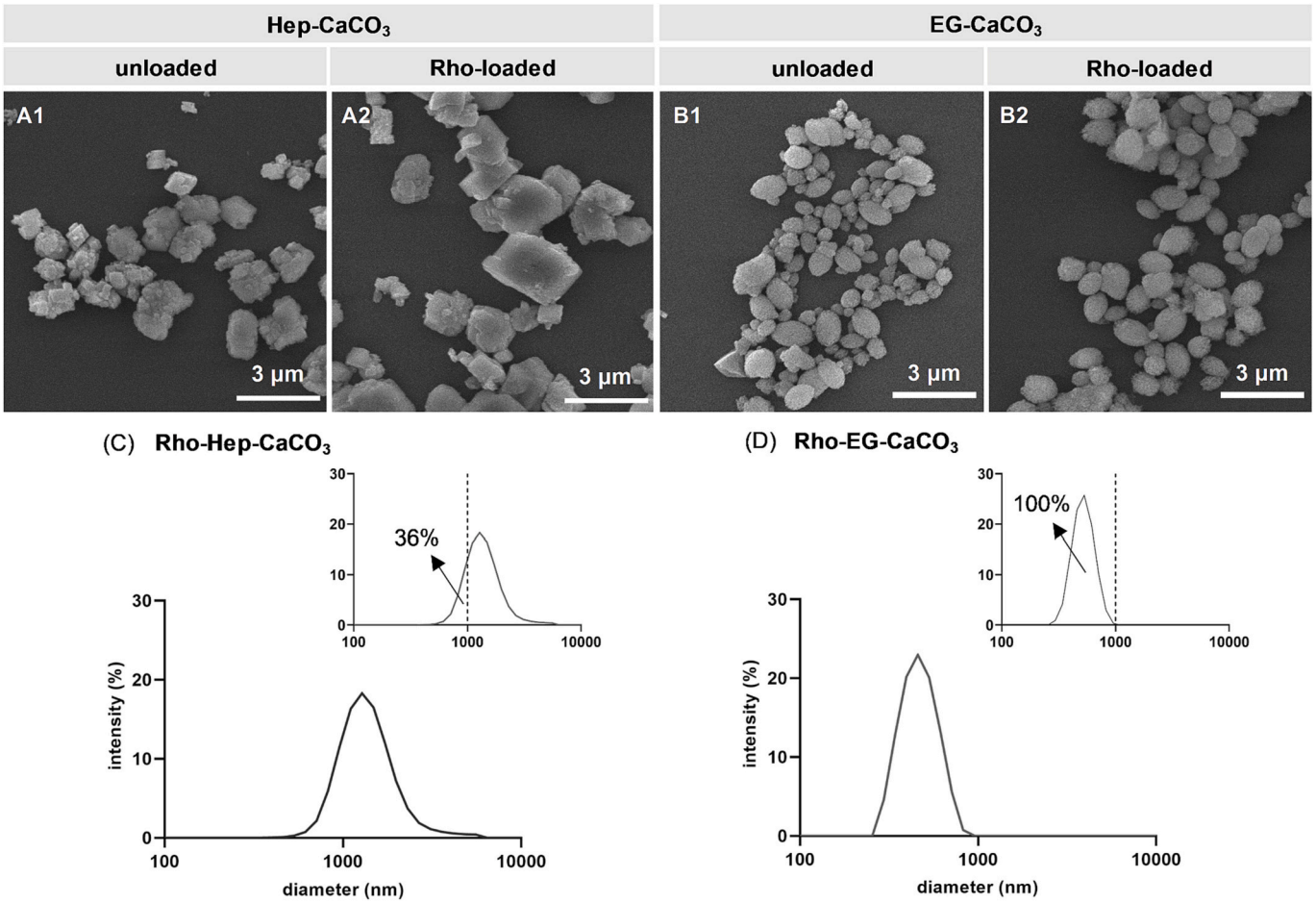

Fig. 2. SEM micrographs of Hep-$CaCO_3$ (A) and EG-$CaCO_3$ (B) without (A1, B1) and with (A2, B2) Rho. Size distribution of (C) Hep-$CaCO_3$ and (D) EG-$CaCO_3$ loaded with Rho. The main graphs show one representative distribution graph. The insets show the average distribution calculated from 35 measurements.

unloaded EG-$CaCO_3$ particles were ellipsoid with sizes between 400 nm and 1 μm (Fig. 2B1, and Fig. A.6-ii in the Appendix). When Rho was encapsulated, the geometry of the particles remained unaltered (Fig. 2A2, B2). However, a comparison between the sizes of unloaded and loaded nanoparticles showed that the encapsulation of Rho in Hep-$CaCO_3$ resulted in a significant increase of the particles diameter (Fig. 2A2): most of the Rho-loaded particles were above 1 μm (Appendix, Fig. A.6-iii) and only 36 % were in the submicron scale (Fig. 2C). On the other hand, the size of EG-$CaCO_3$ was not altered significantly after Rho encapsulation (Fig. 2B2 and Fig. A.6-iv in the Appendix) and 100 % of all particles had a diameter less than or equal to 1 μm (Fig. 2D). We therefore selected EG-$CaCO_3$ nanoparticles for the following experiments.

3.2. Layer-by-layer coating and rhodamine release

Rho-loaded EG-$CaCO_3$ nanoparticles (ζ-potential about −6 mV) served as templates for the assembly of a LbL coating that confers CD44 targeting and regulates the release rate. Up to three bilayers of PLL and HA were assembled. The polyanionic HA was the bioactive building block in this composition, whereas PLL was employed as a polycation that allowed electrostatic stabilization of the LbL build-up. The deposition of PLL and HA was confirmed by the variation of particles charge (Fig. 3A).

We did not find an inversion of the sign of the ζ-potential value after the first bilayer was assembled (*i.e.,* ζ-potential increased upon PLL deposition but did not become positive). This behaviour indicates that PLL compensated the HA charge partially and that the LbL assembly of these two materials does not rely exclusively on electrostatic interactions. These results agree with previous data showing partial compensation of PLL charge by HA and involvement of other supramolecular interactions in the assembly of this polyelectrolyte pair (*e.g.,* hydrogen bonds) [29,48,49].

The Rho release from uncoated and LbL-coated nanoparticles was studied at an acidic pH (pH = 6.3) to mimic the TME. The studied timeframe was selected based on the cell studies: we aimed to determine experimentally the Rho released in the culture medium after supplementation with the nanoparticles. We used nanoparticles coated with only one PLL/HA bilayer because of the long LbL deposition times, *i.e.,* by choosing a low number of layers, the coating time is shortened and a premature release due to long processing times is reduced. After 1 h, uncoated EG-$CaCO_3$ released 16 % of Rho, while only 4 % of Rho was released from the LbL-coated nanoparticles for the same period (Fig. 3B). Within 1 day, these values increased to 65 % and 17 %, respectively, and to 70 % and 30 % within 3 days. After this period, the release did not change substantially. Such a difference (>2-fold) confirms that one PLL/HA bilayer was sufficient to slow the release. It is likely that the coating worked not only as a physical barrier between the nanoparticles and the medium but also as a buffer protecting them against dissolution. Of note, the release at pH = 7.4 was significantly lower than at acidic conditions: only 10 % of Rho was released from the coated nanoparticles after 3 days, evidencing the expected pH response from $CaCO_3$ systems (Appendix, Fig. A.7).

The release profiles were established by fitting the data to different drug release models (Appendix, Fig. A.8). The Rho release from uncoated EG-$CaCO_3$ followed a first-order model ($r^2 = 0.9291$). A release of this type indicates that the diffusion rate of Rho from the nanoparticles is driven mainly by its concentration. However, for the LbL-coated nanoparticles we found a better approximation to the Korsmeyer-Peppas model ($r^2 = 0.7563$), which is indicative of a release that is also affected by the properties of the dynamic polymeric systems (*e.g.,* swelling, erosion, other relaxation/contraction phenomena affecting Rho distribution). Since our LbL coatings are of polymeric nature, Rho must diffuse across this additional barrier and thus the release agrees with the Korsmeyer-Peppas model interpretation. It also confirms the role of LbL in controlling the amount of released Rho over time, which is consistent with the data obtained for other LbL-coated $CaCO_3$ particles [50]. With such an approximation, we can estimate that it would take 91 days for 70 % of Rho to be released (*i.e.,* the same amount released from uncoated nanoparticles after 3 days, Fig. A.9 in the Appendix).

3.3. Interaction of EG-$CaCO_3$ nanoparticles with breast cancer cells

The biological impact of uncoated and LbL-coated EG-$CaCO_3$ nanoparticles was investigated on epithelial breast cancer cells with different CD44 expressions. MDA-MB-231 cells have an aggressive and invasive phenotype and overexpress CD44, while SK-BR-3 cells have a basal expression of this receptor and are considered non-invasive [51–54]. MCF10A cells are used as a model for normal human mammary epithelial cells and have a low CD44 expression, mainly detected in the

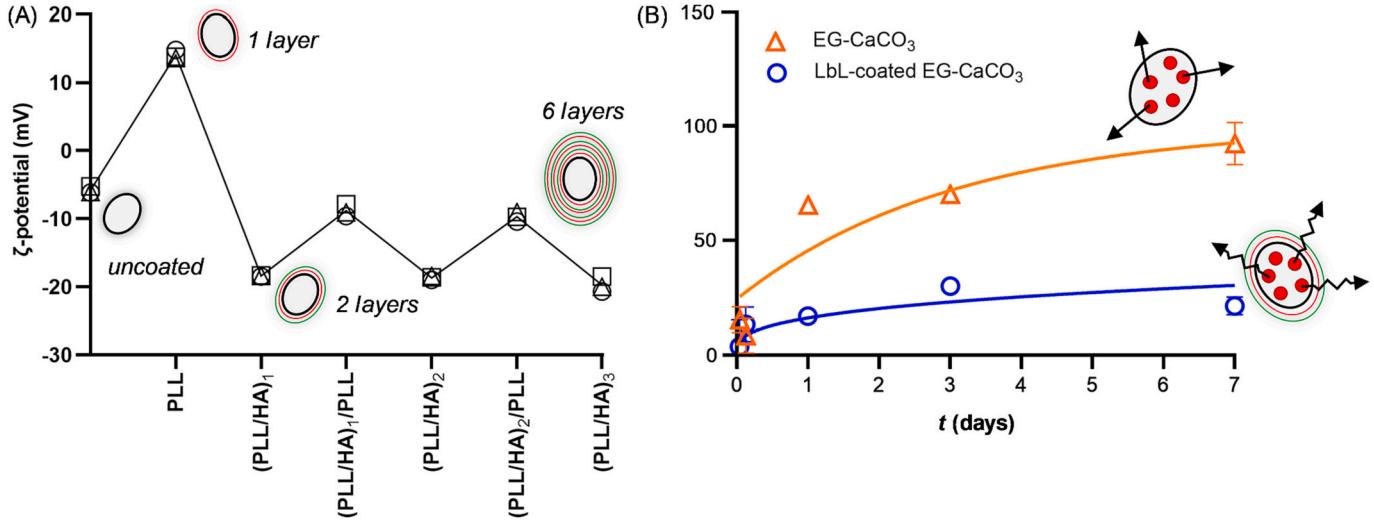

Fig. 3. (A) Zeta-potential change of Rho-loaded EG-$CaCO_3$ nanoparticles upon layer-by-layer deposition. The cartoons represent nanoparticles coated with incremental numbers of layers. Three individual measurements are represented per layer. The line is a visual guide for the variation of the average zeta-potential values. (B) Cumulative release of Rho from uncoated (Δ, orange) and LbL-coated EG-$CaCO_3$ (○, blue) nanoparticles at pH 6.3 for 7 days. The curves are fittings to first-order (uncoated) and Korsmeyer-Peppas (coated) release models. Data are means ± one standard deviation. Some error bars are too small to be seen. The cartoons depict a "fast" release of Rho directly to the medium and a "slow" release across the LbL coating.

cytoplasm [55–57]. We assessed the cytotoxicity of EG-$CaCO_3$ with and without LbL coating and found no cytotoxic effect for the tested cell lines (Fig. 4A–C and Fig. A.10 in the Appendix).

Despite the cells being alive, their metabolism was affected by the nanoparticles (Fig. 4D–E). The metabolic activity of MDA-MB-231 and SK-BR-3 cells significantly decreased with culture time when compared to the control. After 2 days of incubation with the uncoated EG-$CaCO_3$ nanoparticles, the metabolic activity of MDA-MB-231 (70.4 %) and SK-BR-3 cells (81.2 %) decreased, whereas MCF10A cells (88.7 %) were not affected significantly. At day 3, the decrease in the metabolic activity of MDA-MB-231 and SK-BR-3 cells decreased further (64.4 % and 73.4 %, respectively), showing that these nanoparticles affect both phenotypes.

This effect was partially mitigated by the LbL coating after a short culture period (1 day). At longer culture times (2 and 3 days), we observed a decrease in metabolic activity for the breast cancer cell lines but not for the normal cell line, MCF10A, *i.e.,* the effect was similar to the uncoated particles. This delay in the response can be due to different interactions between cells and the coated nanoparticles that trigger different internalization mechanisms, when compared with uncoated particles, and/or different rates of particle dissolution in the lysosome, as shown by the Rho release data.

To analyse the nanoparticles' distribution in the pericellular space and in the cells' cytoplasm we observed the cultures by CLSM (Fig. 5 and Figs. A.11 and A.12 in the Appendix). After 1 day, uncoated EG-$CaCO_3$

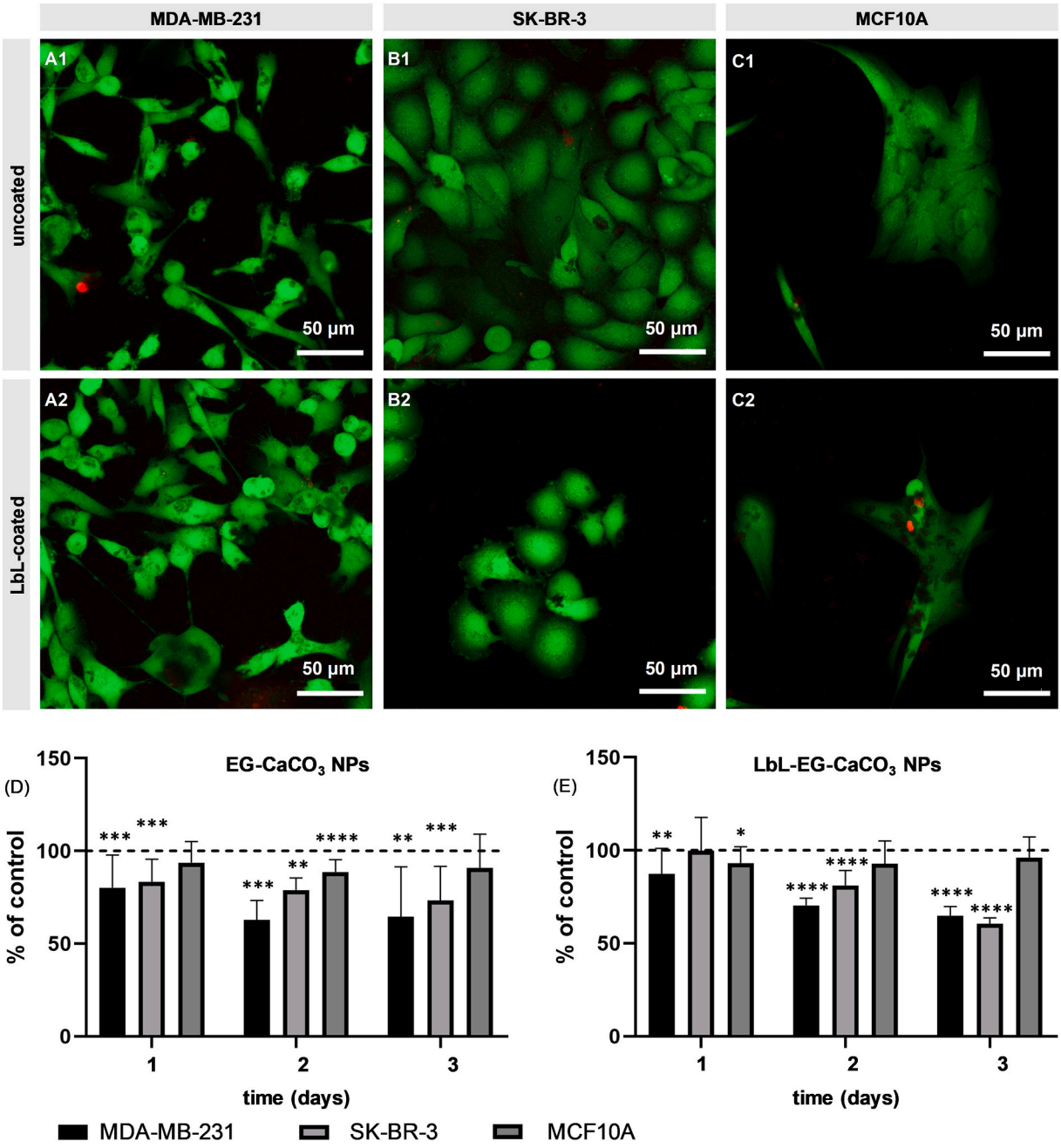

Fig. 4. Live/dead assay of (A) MDA-MB-231, (B) SK-BR-3, and (C) MCF10A cell lines incubated with uncoated and LbL-coated EG-$CaCO_3$ nanoparticles for 3 days (green: live; red: dead). (D, E) Effect of uncoated and LbL-coated EG-$CaCO_3$ nanoparticles (NPs) on metabolic activity of MDA-MB-231, SK-BR-3 and MCF10A cell lines after 1, 2 and 3 days of incubation. Data are presented as a percentage of control (*i.e.,* cells cultured without nanoparticles, dashed line corresponds to the control). Statistical differences are represented between each sample and its control for the different days with $n = 3$. Significant differences are indicated ($^{*}p < 0.05$; $^{**}p < 0.01$; $^{***}p < 0.001$).

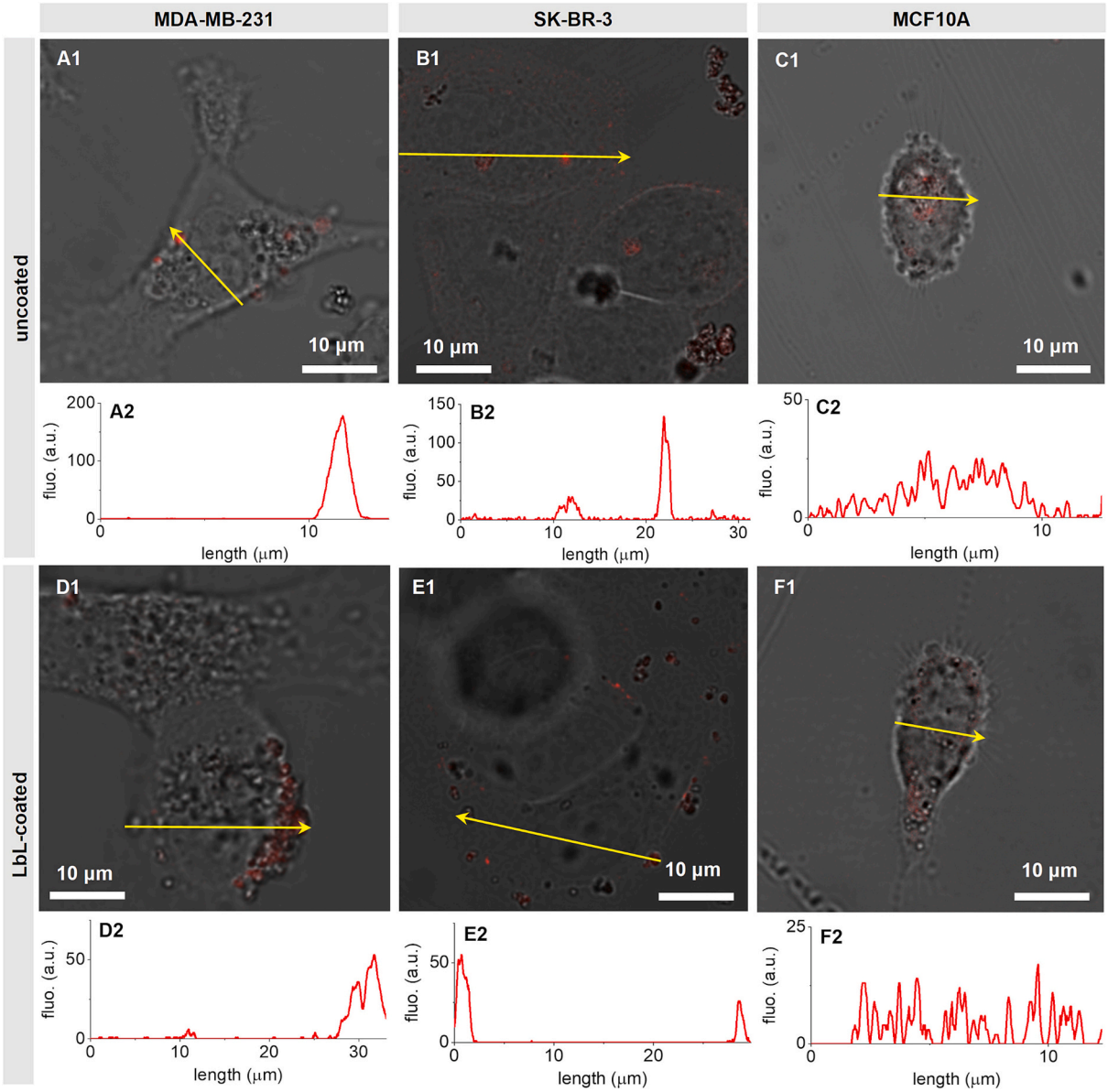

Fig. 5. Distribution of uncoated and LbL-coated EG-$CaCO_3$ nanoparticles after 3 days of incubation with (A, D) MDA-MB-231, (B, E) SK-BR-3, and (C, F) MCF10A cell lines (red: Rho). The plots show the red intensity profiles across the traced yellow lines confirming the distribution of Rho-loaded EG-$CaCO_3$ nanoparticles in the pericellular space or in the cells' cytoplasm. The images and profiles were taken from the CLSM focal plane in the middle of the cells.

nanoparticles were found mainly around the cells, with very few internalized. On days 2 and 3, internalization was observed for all studied cell types, regardless of the CD44 expression level. The results for the LbL-coated EG-$CaCO_3$ nanoparticles were different: most of the particles remained attached to MDA-MB-231 and SK-BR-3 cancer cells, even after 3 days, with only a few being internalized. The red intensity profile across the cancer cells confirmed the predominant presence of uncoated nanoparticles in the cytoplasm (Fig. 5A1, B1) and LbL-coated nanoparticles overlapping with the membrane (Fig. 5D1, E1).

Because we did not observe differences between MDA-MB-231 and SK-BR-3 cells (different expression of CD44), we hypothesized that the endogenous HA creates a protective pericellular coat that engages the expressed CD44 and retains the coated nanoparticles [58]. Lectin binding experiments showed higher HA deposition in the pericellular matrix of MDA-MB-231 cells than in the matrix of SK-BR-3 cells and mainly intracellular HA deposition in the case of MCF10A cells (Appendix, Fig. A.13). Indeed, we observed more nanoparticles around MDA-MB-231 than around SK-BR-3 cells, which agrees with the ticker HA coat around MDA-MB-231 when compared to SK-BR-3 [59].

To understand if CD44 was involved in the internationalization of the nanoparticles, we blocked this receptor before incubating the cells with the nanoparticles. Upon CD44 blocking, we observed enhanced internalization of uncoated and coated nanoparticles by all studied cell types after 24 h (Fig. 6). Interestingly, this enhanced internalization was concomitant with the different distribution of the non-internalized coated nanoparticles in the pericellular space of cancer cells: they were organized in discrete clusters (Fig. 6B2, D2) but not homogeneously distributed as observed for cells without CD44 blocking (Fig. 6B4, D4). This difference was very pronounced for MDA-MB-231 cells. On the one hand, CD44 blocking can affect HA turnover and compromise the HA coating around the cells. On the other hand, we have recently demonstrated that the receptor for hyaluronan mediated motility (RHAMM) can compensate the blocked CD44 and make cells more sensitive to exogenous supplemented HA [47]. These results show that although CD44 receptors are not directly involved in the internalization of the nanoparticles, their presence is important because of their

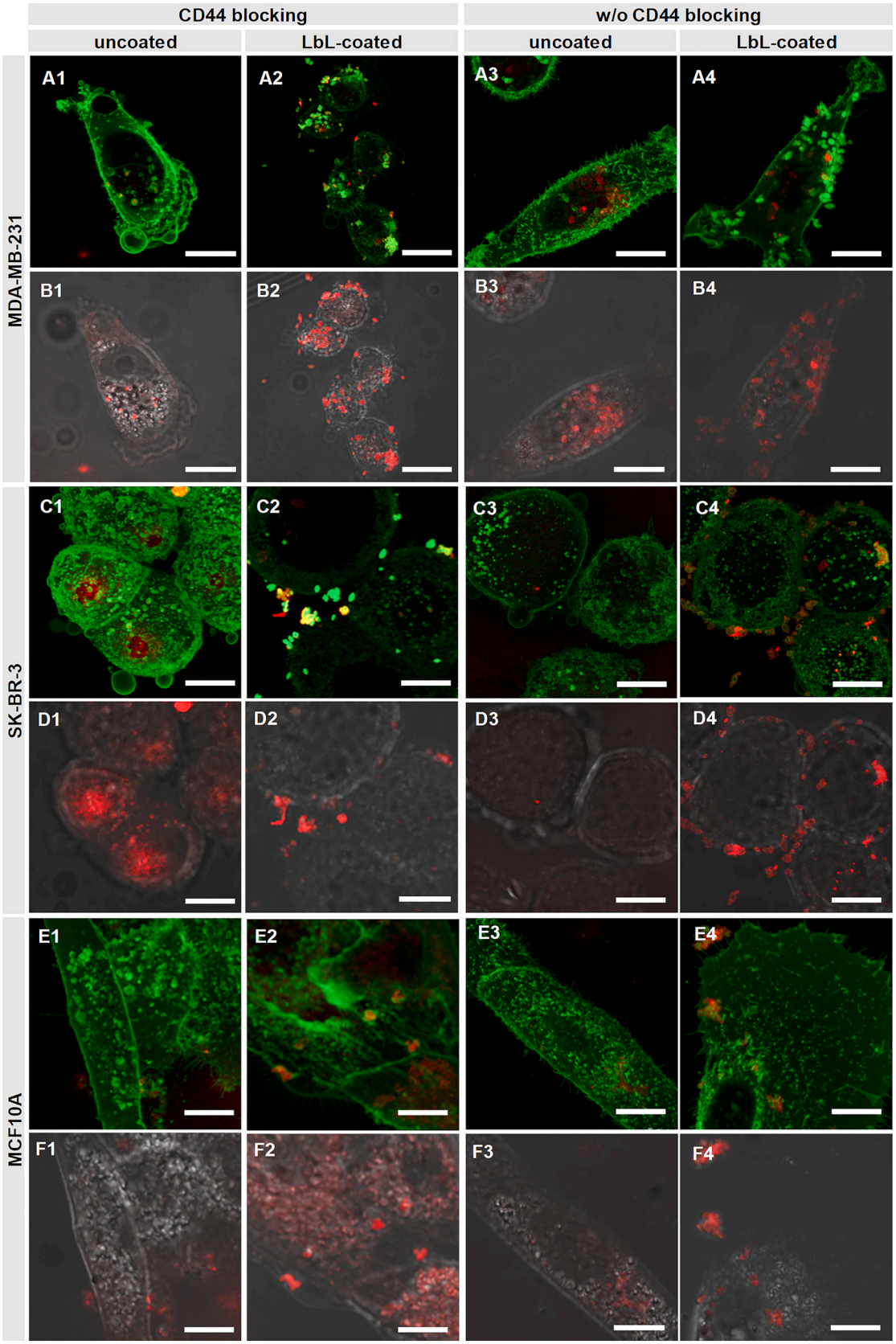

Fig. 6. Distribution of uncoated and LbL-coated EG-$CaCO_3$ nanoparticles after 24 h of incubation with (A, B) MDA-MB-231, (C, D) SK-BR-3, and (E, F) MCF10A cell lines with and without CD44 blocking (red: Rho, green: cell membrane glycoproteins). Scale bars: 10 μm.

interactions with endogenous HA.

4. Conclusions

We demonstrated that $CaCO_3$ nanoparticles are a promising platform for the treatment of breast cancer because of their pH responsiveness and negative charge that allows LbL deposition. $CaCO_3$ can be synthesized using a wide variety of techniques. Of all the tested formulations, the adopted approach of using EG as an additive resulted in submicrometric particles that can be potentially internalized by cells. This additive does not compromise the pH responsiveness of $CaCO_3$, as the release of the encapsulated agent remained higher at acidic conditions than at neutral pH. The LbL coating controls the rate of $CaCO_3$ resorption at acidic pH – and thus the release of the encapsulated agent – but also discriminates the nanoparticles interactions with cancer cells and non-tumorigenic cells: LbL coating favours the pericellular immobilization of nanoparticles over their internalization by cells with HA-rich matrix typical for cancer cells.

While we did not contemplate the use of therapeutic drugs, they can be loaded on demand during $CaCO_3$ co-precipitation, converting the nanoparticles into drug delivery systems. We envisage that the enhanced release observed at acidic conditions can be used as a delivery method for chemotherapeutics in the breast cancer tumour environment, *i.e.*, it is possible to reduce the off-site delivery, the development of drug resistances, and the systemic side effects that are common for non-localized treatments. The observed pericellular immobilization offers the possibility of a multimodal breast cancer treatment when combined with the pH responsiveness of $CaCO_3$ systems: specific surface receptors overexpressed in tumours can be targeted and minimize unspecific delivery to healthy cells even further. Moreover, we suggest that future studies should focus on understanding the role of different HA receptors, such as RHAMM, in nanoparticles accumulation in the extracellular matrix.

CRediT authorship contribution statement

Filipa R. Bastos: Validation, Formal Analysis, Investigation, Data Curation, Writing - Original Draft, Writing - Reviewing & Editing, Visualization. **Diana Soares da Costa:** Validation, Formal analysis, Investigation, Data curation, Writing - Reviewing & Editing, Visualization. **Rui** L. **Reis:** Resources, Supervision, Funding Acquisition. **Natália M. Alves:** Conceptualization, Validation, Resources, Writing - Reviewing & Editing, Supervision. **Iva Pashkuleva:** Conceptualization, Methodology, Validation, Resources, Writing - Reviewing & Editing, Supervision, Project Administration. **Rui R. Costa:** Conceptualization, Methodology, Validation, Formal analysis, Investigation, Resources, Data Curation, Writing - Reviewing & Editing, Visualization, Project Administration.

Declaration of competing interest

The authors declare that they have no known competing financial interests or personal relationships that could have appeared to influence the work reported in this paper.

Data availability

Data will be made available on request.

Acknowledgements

This work was supported by the Fundação para a Ciência e Tecnologia (project OncoNeoTreat, grant number PTDC/CTM-REF/0022/2020, co-financed by FCT – OE component); and the European program FEDER/FEEI. R.R.C. acknowledges FCT for support through grants 2022.00764.CEECIND and CEECIND/02842/2017. D.S.C. thanks FCT for the grant SFRH/BPD/85790/2012. Parts of Fig. A.1 were drawn by using pictures from Servier Medical Art. Servier Medical Art by Servier is licensed under a Creative Commons Attribution 3.0 Unported License (https://creativecommons.org/licenses/by/3.0/).

Appendix A. Supplementary data

Supplementary data to this article can be found online at https://doi.org/10.1016/j.bioadv.2023.213563.

References

[1] H. Sung, J. Ferlay, R.L. Siegel, M. Laversanne, I. Soerjomataram, A. Jemal, F. Bray, Global Cancer Statistics, GLOBOCAN estimates of incidence and mortality worldwide for 36 cancers in 185 countries, CA Cancer J. Clin. 71 (2021) (2020) 209–249, https://doi.org/10.3322/caac.21660.
[2] R. Erber, A. Hartmann, Histology of luminal breast Cancer, Breast Care 15 (2020) 327–336, https://doi.org/10.1159/000509025.
[3] S. Loibl, P. Poortmans, M. Morrow, C. Denkert, G. Curigliano, Breast cancer, Lancet 397 (2021) 1750–1769, https://doi.org/10.1016/S0140-6736(20)32381-3.
[4] L. Yin, J.-J. Duan, X.-W. Bian, S.-C. Yu, Triple-negative breast cancer molecular subtyping and treatment progress, Breast Cancer Res. 22 (2020) 61, https://doi.org/10.1186/s13058-020-01296-5.
[5] H.E. Lee, J.H. Kim, Y.J. Kim, S.Y. Choi, S.W. Kim, E. Kang, I.Y. Chung, I.A. Kim, E. J. Kim, Y. Choi, H.S. Ryu, S.Y. Park, An increase in cancer stem cell population after primary systemic therapy is a poor prognostic factor in breast cancer, Br. J. Cancer 104 (2011) 1730–1738, https://doi.org/10.1038/bjc.2011.159.
[6] P.A. Williams, S. Cao, D. Yang, R.L. Jennelle, Patient-reported outcomes of the relative severity of side effects from cancer radiotherapy, Support Care Cancer 28 (2020) 309–316, https://doi.org/10.1007/s00520-019-04820-2.
[7] Q. Liu, J. Qiu, Q. Lu, Y. Ma, S. Fang, B. Bu, L. Song, Comparison of endocrine therapy and chemotherapy as different systemic treatment modes for metastatic luminal HER2-negative breast cancer patients —a retrospective study, Front. Oncol. 12 (2022), 873570, https://doi.org/10.3389/fonc.2022.873570.
[8] Y. Xie, X. Du, Y. Zhao, C. Gong, S. Hu, S. You, S. Song, X. Hu, Z. Yang, B. Wang, Chemotherapy shows a better efficacy than endocrine therapy in metastatic breast Cancer patients with a heterogeneous estrogen receptor expression assessed by 18F-FES PET, Cancers 14 (2022) 3531, https://doi.org/10.3390/cancers14143531.
[9] M. Chen, C. Chen, Z. Shen, X. Zhang, Y. Chen, F. Lin, X. Ma, C. Zhuang, Y. Mao, H. Gan, P. Chen, X. Zong, R. Wu, Extracellular pH is a biomarker enabling detection of breast cancer and liver cancer using CEST MRI, Oncotarget 8 (2017) 45759–45767, https://doi.org/10.18632/oncotarget.17404.
[10] P. Swietach, R.D. Vaughan-Jones, A.L. Harris, A. Hulikova, The chemistry, physiology and pathology of pH in cancer, Philos. Trans. R. Soc. B 369 (2014) 20130099, https://doi.org/10.1098/rstb.2013.0099.
[11] Y. Zhang, Y. Takahashi, S.P. Hong, F. Liu, J. Bednarska, P.S. Goff, P. Novak, A. Shevchuk, S. Gopal, I. Barozzi, L. Magnani, H. Sakai, Y. Suguru, T. Fujii, A. Erofeev, P. Gorelkin, A. Majouga, D.J. Weiss, C. Edwards, A.P. Ivanov, D. Klenerman, E.V. Sviderskaya, J.B. Edel, Y. Korchev, High-resolution label-free 3D mapping of extracellular pH of single living cells, Nat. Commun. 10 (2019) 5610, https://doi.org/10.1038/s41467-019-13535-1.
[12] Z. Dong, L. Feng, W. Zhu, X. Sun, M. Gao, H. Zhao, Y. Chao, Z. Liu, CaCO3 nanoparticles as an ultra-sensitive tumor-pH-responsive nanoplatform enabling real-time drug release monitoring and cancer combination therapy, Biomaterials 110 (2016) 60–70, https://doi.org/10.1016/j.biomaterials.2016.09.025.
[13] D.B. Trushina, T.N. Borodina, S. Belyakov, M.N. Antipina, Calcium carbonate vaterite particles for drug delivery: advances and challenges, Mater. Today Adv. 14 (2022), 100214, https://doi.org/10.1016/j.mtadv.2022.100214.
[14] C. Xu, Y. Yan, J. Tan, D. Yang, X. Jia, L. Wang, Y. Xu, S. Cao, S. Sun, Biodegradable nanoparticles of polyacrylic acid–stabilized amorphous CaCO3 for tunable pH-responsive drug delivery and enhanced tumor inhibition, Adv. Funct. Mater. 29 (2019) 1808146, https://doi.org/10.1002/adfm.201808146.
[15] V.L. Kudryavtseva, L. Zhao, S.I. Tverdokhlebov, G.B. Sukhorukov, Fabrication of PLA/CaCO3 hybrid micro-particles as carriers for water-soluble bioactive molecules, Colloids Surf., B 157 (2017) 481–489, https://doi.org/10.1016/j.colsurfb.2017.06.011.
[16] A.I. Petrov, D.V. Volodkin, G.B. Sukhorukov, Protein—calcium carbonate Coprecipitation: a tool for protein encapsulation, Biotechnol. Prog. 21 (2005) 918–925, https://doi.org/10.1021/bp0495825.
[17] J.J. Richardson, J.W. Maina, H. Ejima, M. Hu, J. Guo, M.Y. Choy, S.T. Gunawan, L. Lybaert, C.E. Hagemeyer, B.G. De Geest, F. Caruso, Versatile loading of diverse cargo into functional polymer capsules, Adv. Sci. 2 (2015) 1400007, https://doi.org/10.1002/advs.201400007.
[18] S.A. Kamba, M. Ismail, S.H. Hussein-Al-Ali, T.A.T. Ibrahim, Z.A.B. Zakaria, In vitro delivery and controlled release of doxorubicin for targeting osteosarcoma bone cancer, Molecules 18 (2013) 10580–10598, https://doi.org/10.3390/molecules180910580.
[19] C. Wang, S. Chen, Y. Wang, X. Liu, F. Hu, J. Sun, H. Yuan, Lipase-triggered water-responsive "Pandora's box" for cancer therapy: toward induced neighboring effect and enhanced drug penetration, Adv. Mater. 30 (2018) 1706407, https://doi.org/10.1002/adma.201706407.

[20] D. Alkekhia, P.T. Hammond, A. Shukla, Layer-by-layer biomaterials for drug delivery, Annu. Rev. Biomed. Eng. 22 (2020) 1–24, https://doi.org/10.1146/annurev-bioeng-060418-052350.

[21] R.R. Costa, J.F. Mano, Polyelectrolyte multilayered assemblies in biomedical technologies, Chem. Soc. Rev. 43 (2014) 3453–3479, https://doi.org/10.1039/C3CS60393H.

[22] C. Monge, J. Almodóvar, T. Boudou, C. Picart, Spatio-temporal control of LbL films for biomedical applications: from 2D to 3D, Adv. Healthcare Mater. 4 (2015) 811–830, https://doi.org/10.1002/adhm.201400715.

[23] F. Ali Said, N. Bousserrhine, V. Alphonse, L. Michely, S. Belbekhouche, Antibiotic loading and development of antibacterial capsules by using porous CaCO3 microparticles as starting material, Int. J. Pharm. 579 (2020), 119175, https://doi.org/10.1016/j.ijpharm.2020.119175.

[24] C. Tan, C. Dima, M. Huang, E. Assadpour, J. Wang, B. Sun, M.S. Kharazmi, S. M. Jafari, Advanced CaCO3-derived delivery systems for bioactive compounds, Adv. Colloid Interf. Sci. 309 (2022), 102791, https://doi.org/10.1016/j.cis.2022.102791.

[25] M. Lintuluoto, Y. Horioka, S. Hongo, J.M. Lintuluoto, Y. Fukunishi, Molecular dynamics simulation study on allosteric regulation of CD44-Hyaluronan binding as a force sensing mechanism, ACS Omega 6 (2021) 8045–8055, https://doi.org/10.1021/acsomega.0c05502.

[26] A.M. Carvalho, R. Teixeira, R. Novoa-Carballal, R.A. Pires, R.L. Reis, I. Pashkuleva, Redox-responsive micellar nanoparticles from Glycosaminoglycans for CD44 targeted drug delivery, Biomacromolecules 19 (2018) 2991–2999, https://doi.org/10.1021/acs.biomac.8b00561.

[27] R. Thapa, G.D. Wilson, The importance of CD44 as a stem cell biomarker and therapeutic target in Cancer, Stem Cells Int. 2016 (2016) 2087204, https://doi.org/10.1155/2016/2087204.

[28] H. Xu, K. Wu, Y. Tian, Q. Liu, N. Han, X. Yuan, L. Zhang, G.S. Wu, K. Wu, CD44 correlates with clinicopathological characteristics and is upregulated by EGFR in breast cancer, Int. J. Oncol. 49 (2016) 1343–1350, https://doi.org/10.3892/ijo.2016.3639.

[29] S. Amorim, I. Pashkuleva, C.A. Reis, R.L. Reis, R.A. Pires, Tunable layer-by-layer films containing hyaluronic acid and their interactions with CD44, J. Mater. Chem. B 8 (2020) 3880–3885, https://doi.org/10.1039/D0TB00407C.

[30] V. Domínguez-Arca, R.R. Costa, A.M. Carvalho, P. Taboada, R.L. Reis, G. Prieto, I. Pashkuleva, Liposomes embedded in layer by layer constructs as simplistic extracellular vesicles transfer model, Mater. Sci. Eng. C 121 (2021), 111813, https://doi.org/10.1016/j.msec.2020.111813.

[31] Y. Ueno, H. Futagawa, Y. Takagi, A. Ueno, Y. Mizushima, Drug-incorporating calcium carbonate nanoparticles for a new delivery system, J. Control. Release 103 (2005) 93–98, https://doi.org/10.1016/j.jconrel.2004.11.015.

[32] B. Parakhonskiy, M.V. Zyuzin, A. Yashchenok, S. Carregal-Romero, J. Rejman, H. Möhwald, W.J. Parak, A.G. Skirtach, The influence of the size and aspect ratio of anisotropic, porous CaCO3 particles on their uptake by cells, J. Nanobiotechnol. 13 (2015) 53, https://doi.org/10.1186/s12951-015-0111-7.

[33] Y.-C. Chen, W.-T. Chiu, C. Chang, P.-C. Wu, T.-Y. Tu, H.-P. Lin, H.-C. Chang, Chemo-photothermal effects of doxorubicin/silica–carbon hollow spheres on liver cancer, RSC Adv. 8 (2018) 36775–36784, https://doi.org/10.1039/C8RA08538B.

[34] H. Kim, D.J. Burgess, Effect of drug stability on the analysis of release data from controlled release microspheres, J. Microencapsul. 19 (2002) 631–640, https://doi.org/10.1080/02652040210140698.

[35] S.M. Lombardo, N. Günday Türeli, M. Koch, M. Schneider, A.E. Türeli, Reliable release testing for nanoparticles with the NanoDis system, an innovative sample and separate technique, Int. J. Pharm. 609 (2021), 121215, https://doi.org/10.1016/j.ijpharm.2021.121215.

[36] M. Yu, W. Yuan, D. Li, A. Schwendeman, S.P. Schwendeman, Predicting drug release kinetics from nanocarriers inside dialysis bags, J. Control. Release 315 (2019) 23–30, https://doi.org/10.1016/j.jconrel.2019.09.016.

[37] A. Celebioglu, T. Uyar, Design of polymer-free vitamin-a acetate/cyclodextrin nanofibrous webs: antioxidant and fast-dissolving properties, Food Funct. 11 (2020) 7626–7637, https://doi.org/10.1039/D0FO01776K.

[38] J. Schindelin, I. Arganda-Carreras, E. Frise, V. Kaynig, M. Longair, T. Pietzsch, S. Preibisch, C. Rueden, S. Saalfeld, B. Schmid, J.-Y. Tinevez, D.J. White, V. Hartenstein, K. Eliceiri, P. Tomancak, A. Cardona, Fiji: an open-source platform for biological-image analysis, Nat. Methods 9 (2012) 676–682, https://doi.org/10.1038/nmeth.2019.

[39] Y.-Q. Niu, J.-H. Liu, C. Aymonier, S. Fermani, D. Kralj, G. Falini, C.-H. Zhou, Calcium carbonate: controlled synthesis, surface functionalization, and nanostructured materials, Chem. Soc. Rev. 51 (2022) 7883–7943, https://doi.org/10.1039/D1CS00519G.

[40] L.M.I. Schijven, V. Saggiomo, A.H. Velders, J.H. Bitter, C.V. Nikiforidis, On the influence of protein aggregate sizes for the formation of solid and hollow protein microparticles, J. Colloid Interface Sci. 631 (2023) 181–190, https://doi.org/10.1016/j.jcis.2022.11.007.

[41] D.V. Volodkin, A.I. Petrov, M. Prevot, G.B. Sukhorukov, Matrix polyelectrolyte microcapsules: new system for macromolecule encapsulation, Langmuir 20 (2004) 3398–3406, https://doi.org/10.1021/la036177z.

[42] G. Yan, Y. Feng, Z. Gao, X. Zeng, W. Hong, W. Liu, Y. Sun, X. Tang, T. Lei, L. Lin, Stable and biocompatible cellulose-based CaCO3 microspheres for tunable pH-responsive drug delivery, ACS Sustain. Chem. Eng. 7 (2019) 19824–19831, https://doi.org/10.1021/acssuschemeng.9b05144.

[43] S.Y.M.H. Seepma, S.E. Ruiz-Hernandez, G. Nehrke, K. Soetaert, A.P. Philipse, B.W. M. Kuipers, M. Wolthers, Controlling CaCO3 particle size with {Ca2+}:{CO32–} ratios in aqueous environments, Cryst. Growth Des. 21 (2021) 1576–1590, https://doi.org/10.1021/acs.cgd.0c01403.

[44] I. Capila, R.J. Linhardt, Heparin–protein interactions, Angew. Chem., Int. Ed. 41 (2002) 390–412, doi: 10.1002/1521-3773(20020201)41:3<390::AID-ANIE390>3.0.CO;2-B.

[45] R.J. Weiss, J.D. Esko, Y. Tor, Targeting heparin and heparan sulfate protein interactions, Org. Biomol. Chem. 15 (2017) 5656–5668, https://doi.org/10.1039/C7OB01058C.

[46] P. Foroozandeh, A.A. Aziz, Insight into cellular uptake and intracellular trafficking of nanoparticles, Nanoscale Res. Lett. 13 (2018) 339, https://doi.org/10.1186/s11671-018-2728-6.

[47] R.A. Boulos, F. Zhang, E.S. Tjandra, A.D. Martin, D. Spagnoli, C.L. Raston, Spinning up the polymorphs of calcium carbonate, Sci. Rep. 4 (2014) 3616, https://doi.org/10.1038/srep03616.

[48] L. Shen, P. Chaudouet, J. Ji, C. Picart, pH-amplified multilayer films based on Hyaluronan: influence of HA molecular weight and concentration on film growth and stability, Biomacromolecules 12 (2011) 1322–1331, https://doi.org/10.1021/bm200070k.

[49] R. Teixeira, R.L. Reis, I. Pashkuleva, Influence of the sulfation degree of glycosaminoglycans on their multilayer assembly with poly-l-lysine, Colloids Surf., B 145 (2016) 567–575, https://doi.org/10.1016/j.colsurfb.2016.05.069.

[50] R.R. Costa, C.A. Custódio, F.J. Arias, J.C. Rodríguez-Cabello, J.F. Mano, Nanostructured and thermoresponsive recombinant biopolymer-based microcapsules for the delivery of active molecules, Nanomedicine 9 (2013) 895–902, https://doi.org/10.1016/j.nano.2013.01.013.

[51] A.M. Carvalho, D. Soares da Costa, R.L. Reis, I. Pashkuleva, RHAMM expression tunes the response of breast cancer cell lines to hyaluronan, Acta Biomater. 146 (2022) 187–196, https://doi.org/10.1016/j.actbio.2022.05.013.

[52] A.M. Carvalho, D. Soares da Costa, R.L. Reis, I. Pashkuleva, Influence of hyaluronan density on the behavior of breast cancer cells with different CD44 expression, Adv. Healthcare Mater. 11 (2022) 2101309, https://doi.org/10.1002/adhm.202101309.

[53] C. Sheridan, H. Kishimoto, R.K. Fuchs, S. Mehrotra, P. Bhat-Nakshatri, C.H. Turner, R. Goulet, S. Badve, H. Nakshatri, CD44+/CD24-breast cancer cells exhibit enhanced invasive properties: an early step necessary for metastasis, Breast Cancer Res. 8 (2006) R59, https://doi.org/10.1186/bcr1610.

[54] N. Sun, H.N. Xu, Q. Luo, L.Z. Li, Potential indexing of the invasiveness of breast Cancer cells by mitochondrial redox ratios, Adv. Exp. Med. Biol. 923 (2016) 121–127, https://doi.org/10.1007/978-3-319-38810-6_16.

[55] J. Puleo, K. Polyak, The MCF10 model of breast tumor progression, Cancer Res. 81 (2021) 4183–4185, https://doi.org/10.1158/0008-5472.CAN-21-1939.

[56] H.D. Soule, T.M. Maloney, S.R. Wolman, W.D. Peterson Jr., R. Brenz, C. M. McGrath, J. Russo, R.J. Pauley, R.F. Jones, S.C. Brooks, Isolation and characterization of a spontaneously immortalized human breast epithelial cell line, MCF-10, Cancer Res. 50 (1990) 6075–6086.

[57] N. Vale, S. Silva, D. Duarte, D.M.A. Crista, L. Pinto da Silva, J.C.G. Esteves da Silva, Normal breast epithelial MCF-10A cells to evaluate the safety of carbon dots, RSC Med. Chem. 12 (2021) 245–253, https://doi.org/10.1039/D0MD00317D.

[58] E.A. Turley, D.K. Wood, J.B. McCarthy, Carcinoma cell Hyaluronan as a "portable" Cancerized Prometastatic microenvironment, Cancer Res. 76 (2016) 2507–2512, https://doi.org/10.1158/0008-5472.CAN-15-3114.

[59] A.M. Carvalho, D. Soares da Costa, P.M.R. Paulo, R.L. Reis, I. Pashkuleva, Co-localization and crosstalk between CD44 and RHAMM depend on hyaluronan presentation, Acta Biomater. 119 (2021) 114–124, https://doi.org/10.1016/j.actbio.2020.10.024.